



Nuclear Materials Authority
P.O.Box 530 Maadi, Cairo, Egypt

DOAJ DIRECTORY OF
OPEN ACCESS
JOURNALS

ISSN 2314-5609
Nuclear Sciences Scientific Journal
9, 55-78
2020
<http://www.ssnma.com>

MINERALOGY AND GEOCHEMISTRY OF A NEW URANIUM OCCURRENCE AT THE DECANT OF WADI EL REDDAH, NORTHEASTERN DESERT, EGYPT

HOSSAM A. KHAMIS; OSAMA A. EBAN and NEVEEN S. ABED

Nuclear Materials Authority , Cairo, Egypt

ABSTRACT

Gattar granites are affected by widespread deuteric and post magmatic hydrothermal activities. Hydrothermal alterations associated U-mineralization in the host granites include hematization, sericitization, episyenitization (desilicification) and fluoritization. Alkali metasomatism is represented by microclinization, sericitization and muscovitization of alkali feldspar and plagioclase. Two new radioactive occurrences were discovered namely GXXIII and GXXIV. The first radioactive occurrence is located 150-180 m from the contact between the Gattarian granite and the Hammamat molasse sediments. The intersection shows highly hematized hallos with deep brown to reddish pink color associating some remarkable silicification. The other radioactive location is controlled by several factors mainly represented by the NE-SW basic dyke of 2-3 m thickness and bound the radioactive spots from the north. This radioactive location is located some 350 m from the GXXIV location and is more than 0.5 Km away from the granite-Hammamat contact zone. The location includes three radioactive spots arranged along major shear zone trending N25E-S25W.

Generally, loss and gain calculations indicate that the altered samples exhibit an increase in total iron, K, Mn, Al, Ca and Mg and decrease in Na, P, Si, L.O.I. and Ti, in addition to elevated contents of Cu, Co, Pb, Cs, Y, Ga, Hf, Sn, V, Nb, Rb, Ta, Th, U, Tl, Zr, W, Zn and depleted in Ba, Sr and Ni. Y/Ho ratios value show complexation with fluorine and carbonates which is confirmed by the presence of fluorite and calcite.

Hydrothermal alteration during late magmatic stage is identified by the unusual Zr/Hf, Sr/Eu, Nb/Ta, La/Nb, La/Ta, Rb/Sr and U/Th ratios. Highly evolved nature of these rocks is also manifested by irregular REE's pattern that is most visible in late magmatic differentiates with strong hydrothermal or deuteric alteration represented with K-metasomatism and fluoritization. Positive correlation of uranium and most of trace and rare earth elements indicate co-mobilization and precipitation of these elements. Microscopic and scanning electron microscopic studies revealed the presence of uranophane, kasolite, cotunite, coronadite, galena, fluorite and amazonite.

INTRODUCTION

Airborne or ground radiometric studies and field investigation done by Nuclear Materials Authority (NMA) resulted into the discovery of many radioactive occurrences in the Eastern Desert, including; El Erediya, Kab Amiri, El Missikat, Rei El Garra, Gattar, among others (Ammar, 1973, El Kassas, 1974, El Taher, 1985 and Salman et al., 1990). All these occurrences were related to Precambrian younger granites. Gabal (G) Gattar granites were subjected to more than one tectonic episode printed on the rock surfaces by joints, faults and shear zones of different attitudes. They were affected by widespread deuteric and post magmatic hydrothermal activities. Hematitization, silicification, episyenitization, fluoritization and epidotization with partial kaolinitization are the most pronounced wall rock alteration features developed.

The differences in the ionic and valences (Ce^{3+} and Ce^{4+} , Eu^{2+} and Eu^{3+}) were the main factors controlled the geochemical behavior of rare earth elements in any geological environment (e.g., Bau, 1996; Pan and Breaks, 1997; Irber, 1999; Monecke et al., 2002). Rare earth elements tetrad effect also could be considered as another factor affecting the REEs distributions (e.g. Masuda et al., 1987; Kawabe, 1995; Bau, 1996; Irber, 1999).

Tetrad effect in some geological environments can be observed as a split of rare earth element (REE) pattern into four rounded segments (i) La–Nd, (ii) Pm–Gd, (iii) Gd–Ho, and (iv) Er–Lu, each tetrad forms a smooth convex or concave pattern (Masuda et al., 1987).

The aim of the present contribution is to investigate the major, trace and rare earth elements geochemistry of Gabal Gattar altered granites and its relation to their mineral association. Also, the wall rock alterations and geochemistry of the isovalents will be studied.

METHODOLOGY

Twenty two samples were collected from

Gattar granite (Fig. 1). These samples are fresh and altered granites. Only three samples represent the highly altered and mineralized granites from the new discovered occurrences. Chemical analyses of the three altered granite samples were carried out in ACME analytical Laboratories of Vancouver, Canada, for major oxides, trace and rare earth elements by inductively coupled plasma-emission spectrometry (ICPES) and ICP-mass spectrometry (ICP-MS). Detection limits for major oxides and trace elements were, respectively, 0.001 wt% to 0.04 wt% and 0.01 to 0.5 ppm. Analytical precision, as calculated from replicate analyses, was 0.5% for major elements and varied from 2% to 20% for trace elements. Mineral separation and identification were carried out at the Laboratories of NMA. The heavy liquids separation technique using bromoform of specific gravity 2.85 gm/cm³ was used to concentrate the heavy minerals. Then, the separation of magnetite was achieved by hand magnet. The heavy mineral fractions were passed through a Frantz isodynamic magnetic to separate the remaining magnetite and produce several magnetic fractions at 0.2, 0.5, 0.7, 1, and 1.5 amperes. Each of these fractions contained its own characteristic minerals. Mineral identification was performed through the Environmental Scanning Electron Microscope (ESEM).

GEOLOGICAL SETTING

Gabal Gattar batholith is located among the basement rocks of the northern part of the Eastern Desert, Egypt (Fig. 2). The area of G. Gattar, in general, includes several rock types: (from the older to the younger) metavolcanics, metagabbro-diorites complex, Hammamat sedimentary rocks, Younger granites (Gattarian granites) and the Post-granitic dykes.

The metavolcanics are mainly represented by scattered and disconnected exposures at the extreme northern and northeastern flank of W. El Reddah (Fig. 3). These are represented by metabasalt, metabasaltic andesite, metaandesite and metadacite as well as well foliated

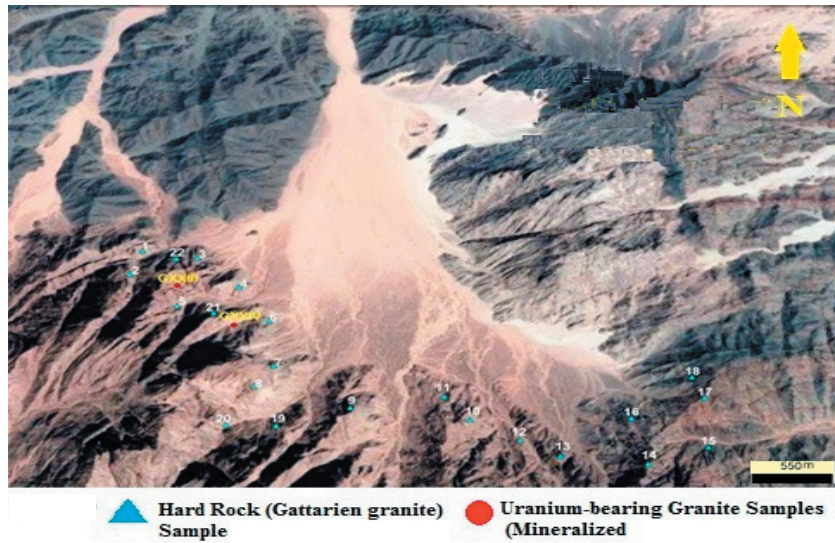


Fig. 1: Landsat TM image of Wadi El Reddah area showing sampling (by white color) and location of the two newly discovered uranium occurrences (by yellow color)

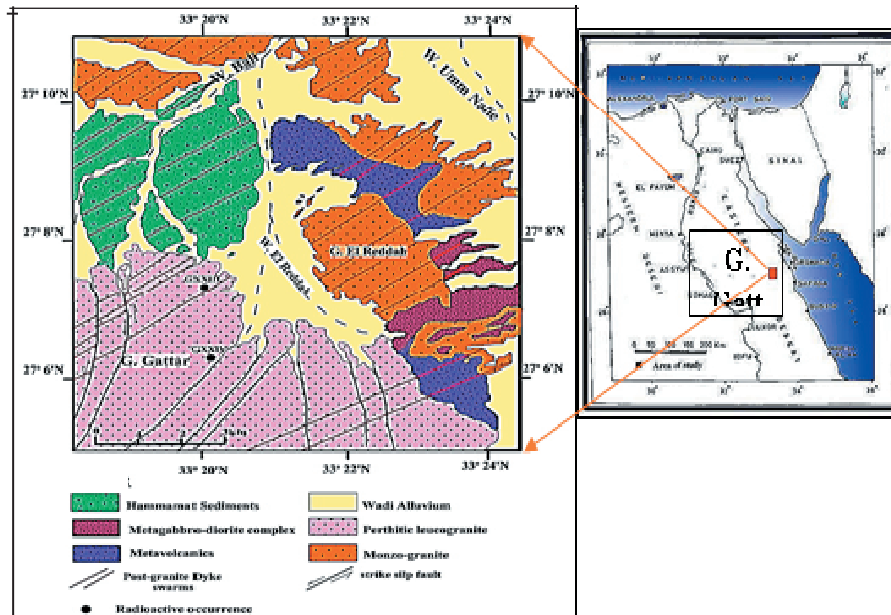


Fig. 2: Regional geological map of G. Gattar and its environs (Modified after El Rakaiby and Shalaby, 1988)



Fig. 3: Photograph showing the metavolcanics rock type

meta-pyroclastics. These exposures represent the remnants of the huge raft (8 km² area) or roof pendant of G. Kehla that lies over and uplifted by G. Gattar granites. The exposures at Wadi (W.) El Reddah are disrupted parts of this big raft. These metavolcanics show, in addition to their regionally metamorphosed characters, a thermal metamorphism by the intrusions of both granites of G. El Reddah and G. Gattar through them.

Two new radioactive occurrences were discovered during the field season 2015-2016 namely GXXIII and GXXIV (Fig.1), (Gattar 23 and Gattar 24) to increase the total number of the discovered occurrences to 24. A brief description for these two radioactive locations will be summarized in as follows:

GXXIII Occurrence

This radioactive occurrence is located 150-180 m from the contact between the Gattarian granite and the Hammamat molasse sediments. The radioactive location is nearly 5m X 3m area, within which several radioactive spots are situated. The radioactive location is controlled by several factors which are the NE-SW basic dyke of 2-3m thickness which bound the radioactive spots from the north.

The location is projected in the side of the dip direction of the basic dyke. The other

controlling factor is the NNE-SSW highly hematitized fracture where its intersection with the NW-SE minor dextral fault mark the location of the radioactive spots. The intersection show highly hematitized hallows with deep brown to reddish pink color with some remarkable silicification. Great similarities between this locations and GVII occurrence.

GXXIV Occurrence

This radioactive location is located some 350m from the GXXIV location and is more than 0.5 Km away from the granite-Hammamat contact zone. The location includes 3 radioactive spots arranged along major shear zone trending N25E-S25W. The mineralization is restricted to 25m length of the total shear zone.

The shear zone show high degree of alterations represented by hematitization, silicification, kaolinitization and the most important is the episyenitization. The episyenite is of a hematitized type at the radioactive spots but the kaolinized type also exists. The intersection of this U-hosting shear zone and the NW-SE fractures show a markable increase in the radioactivity due to the increase of the hematite alteration and the increase of the degree of the episyenitization.

The metagabbro-diorite complex, which has an intimate association with the previously mentioned metavolcanics is located at the southeastern part of W. El Reddah. It is intruded and cut by arms and off-shoots from the north by G. El Reddah monzogranites and from the south and east by the perthitic granite of G. Gattar. The complex frequently carries scattered xenoliths of metavolcanics, metaporphyrites and metapyroclastics. It has a composition ranging from melano-gabbro to diorite and quartz diorites with different grain size (Fig. 4).

The Hammamat sedimentary rocks are exposed along W. El Reddah at its western flank and intruded by the Gattarian granites. These exposures are the southern extension of the



Fig. 4: Photograph showing the metagabbro-diorite complex



Fig. 5: Photograph showing the Hammamat sediments

main G. Umm Tawat basin present along W. Bali. These sediments include the polymictic conglomerates, graywackes and siltstone (Fig. 5). They are of molasses type, and are deposited in intermountain basins, as a result of rapid uplift and erosion in fresh water braided stream and alluvial environment during the late Proterozoic (Grothaus et al., 1979). They are intruded by the younger granite of G. Gattar forming a sharp intrusive contact.

G. El Reddah monzogranite is located along the eastern flank of W. El Reddah. It constitute one circular rounded granitic mass (Fig. 6). This type of granite represents an early phase of younger granites "G2-granites" according to Hussein et al. (1982) classification of the Egyptian granites. It intrudes the metavolcanics exposures at its northern contact sending off-shoots and apophysis and also intrudes the metagabbro-diorite complex at its southern contact taking abundant huge xenoliths. It is medium to coarse grained whitish pink monzogranites or adamalite and the percentage of the K-feldspar slightly exceeds that of plagioclase. Its composition is quite near to that of G. Salaat El Baligh and is considered to be of its extension.

G. Gattar younger granite represents very high rough topographic scenery in North Eastern Desert; 1969 m above sea level (Fig. 7). It has a sharp intrusive contact against the other rock types in the area as well as the



Fig. 6: Photograph showing Gabal El Reddah monzogranite

acidic dykes. It is cut and traversed by the younger basic dyke swarms. This granite is a very good potential uranium prospect where up to 24 uranium occurrences are discovered at its northern sector. It is typical medium grained, hard and massive pink granite characters with extensive wall rock hydrothermal alterations along its fractures and fault zones. According to Hussein et al. (1982) classification of the Egyptian granites, it is referred to as "G3-granites".

Post granitic dyke swarms are spreading all over the area and are represented by bi-modal acidic (older) and basic (younger) dyke swarms while the intermediate dykes are very rare in the area. They cut all the above



Fig. 7: Photograph showing Gabal Gattar younger granites

mentioned rock types along NE-SW parallel direction and can be traced for hundreds of kilometers.

RESULTS

Host-Rock Alteration

It is worthy to mention that the studied Gattarian granites are subjected to more than one stage of hydrothermal alterations (pre-ore alkali-metasomatism and ore stage hydrothermal alteration) (Salem, 2004; El-Feky, 2011; Shalaby et al., 2015). The pronounced alteration process in the discovered occurrence is mainly alkali metasomatism. It is recorded by various types as microclinization, sericitization and muscovitization of alkali feldspar and plagioclase.

Sericitization and muscovitization are clarified by partially sericitized, muscovitized plagioclase and feldspars (Figs. 8-13). Hematitization, episyenitization (desilicification) and fluoritization are the main alteration processes associating the uranium mineralization (Figs. 8-13).

Hematitization is the most distributed alteration features and overlaps most alteration types. It is mainly resulted from the chloritization of biotite and leads to the reddening of feldspars and other minerals. Episyenitization



Fig. 8: Photomicrograph of hematitization and sericitization of perthite, alkali feldspar granite, XPL

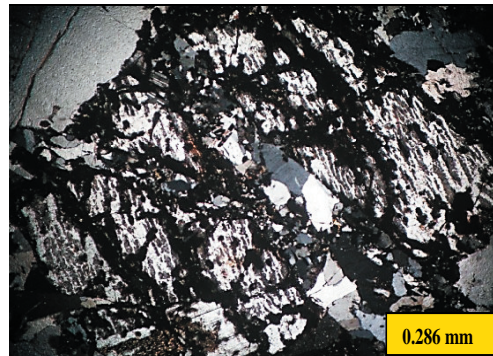


Fig. 9: Photomicrograph of nodular hematitization of string perthite, alkali feldspar granite, XPL

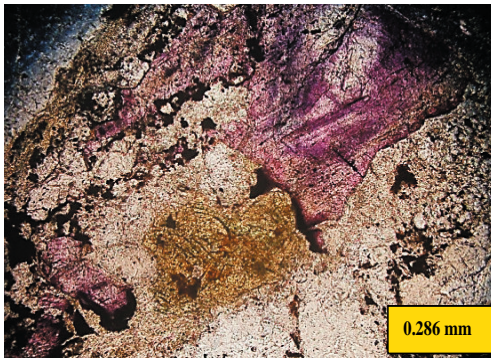


Fig. 10: Photomicrograph of fluorite and secondary uranophane, alkali feldspar granite, XPL

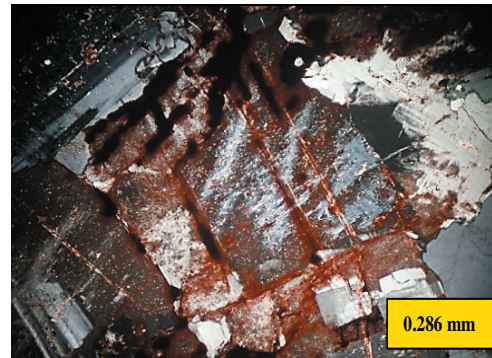


Fig. 13: Photomicrograph of nodular hematitization of flame perthite, alkali feldspar granite, XPL



Fig. 11: Photomicrograph of secondary muscovite associating string perthite, alkali feldspar granite, XPL

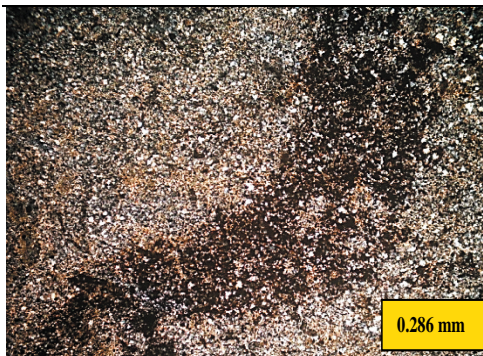


Fig. 12: Photomicrograph of 2^v iron oxide (hematitization) associating sericite, alkali feldspar granite, XPL

of the studied granites is evidenced by dissolution of plagioclase and quartz leaving vugs filled with iron oxides and other radioactive minerals (Figs. 8-13).

Mineralogical Features

The mineralogical investigations are carried out on some representative samples of the mineralized uraniumiferous altered granites. These samples have high uranium and/or thorium contents. They are crushed and mechanically analyzed to obtain the suitable mesh size (-60 & +200 mesh size fraction). Heavy liquid bromoform was used to separate the fractions of the heavy minerals. The separated fractions are then subjected to magnetic separation using Frantz isodynamic separator to separate the heavy minerals according to their magnetic susceptibilities. This was followed by hand picking using the binocular microscope to get rid of the impurities and to obtain pure mineral separates. The picked grains were analyzed by ESEM that gives also semi-quantitative analysis for their elemental composition. The identified radioactive and associated minerals include; uranophane, kasolite, cotunite, coronadite, galena, fluorite and amazonite.

Uranophane [$\text{CaO}(\text{UO}_2)(\text{SiO}_2)(\text{OH})_{25}\text{H}_2\text{O}$]

Uranophane is characterized by various colors as yellow, lemon yellow, greenish

yellow, brownish yellow and orange yellow with different gradations. It occurs as soft aggregates on feldspars or as encrustation, fractures filling and/or coating in the altered K-feldspars. It also occurs as minute crystals arranged in radial tufts or as aggregates of needle like tiny crystals forming fan shape. Their luster is dull and greasy.

Beside Ca, U and Si, some analyses show appreciable amounts of Fe, Pb, Al and K (Fig. 14). Some uranophane crystals show secondary enrichment of Fe. This could be attributed to Fe proxying for Ca in a later phase of mineralized fluids interaction. This is in agreement with Frondel (1958) and Heinrich (1958) who reported appreciable amounts of Fe in the chemical analyses of uranophane. Raslan (2008) identified uraniferous iron grains in Gattar, El Missikat and El Erediya Granites.

Kasolite $\text{Pb}(\text{UO}_2)\text{SiO}_4\cdot\text{H}_2\text{O}$

Kasolite is the only uranyl silicate with major lead ($\text{Pb}(\text{UO}_2)(\text{SiO}_4)\cdot\text{H}_2\text{O}$). It is characterized by its bright colors (canary lemon, yellow and brown of different proportions) and waxy or greasy luster (Fig. 15). Kasolite grains, compared to other uranium secondary minerals are relatively harder (Raslan, 1996). EDX data of the kasolite (Fig. 15) reflect the major element ranges in the Kasolite mineral are U (34.74 - 63.68 wt %), Pb (15.32 - 31.37 wt %) and Si (9.88 - 12.32 wt %), in addition to Ca, Fe, K and Al with less amounts.

Cotunite (PbCl_2)

Cotunite occurs at temperatures below 325°C (Africano et al., 2002). It ranges from colourless to light yellow or light green with adamantine luster and white streak. It occurs as subhedral to anhedral crystals or as inclusion in k-feldspar and fluorite associating sphalerite (Fig. 16). Energy dispersive analyses (EDX) of the studied cotunite indicate that this mineral is mainly composed of Pb and Cl in addition to Al, Si, Ca, Fe, K and F (Fig. 17).

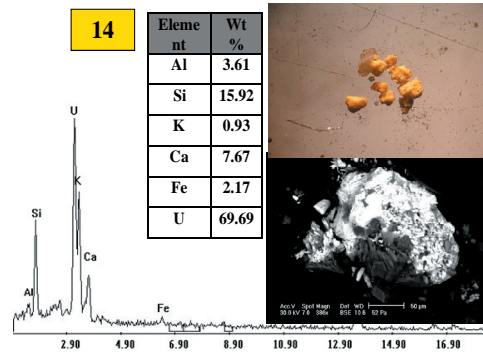


Fig. 14: Binocular photomicrograph, BSE image, EDX analysis of Uranophane from altered granite

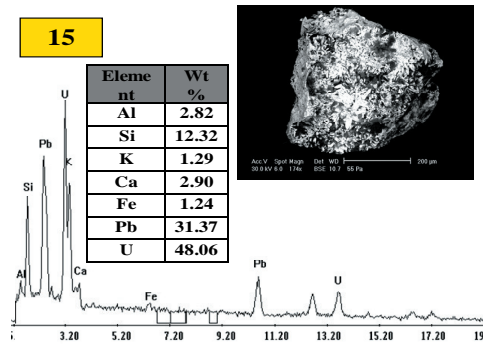


Fig. 15: BSE image, EDX analysis of Kasolite crystal from altered granite

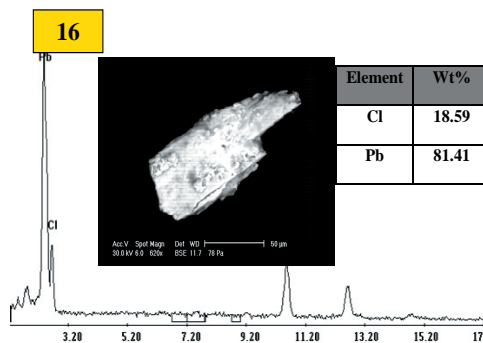


Fig. 16: BSE image, EDX analysis of Cotunite from altered granite

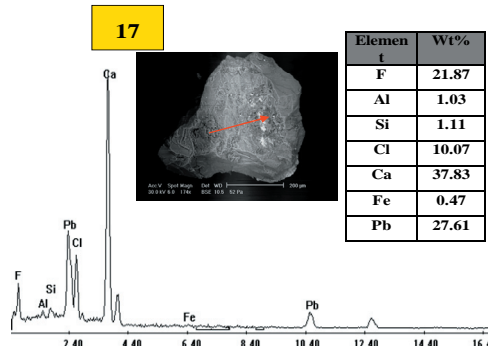


Fig. 17: BSE image, EDX analysis of Cotunite as inclusion on fluorite from altered granite

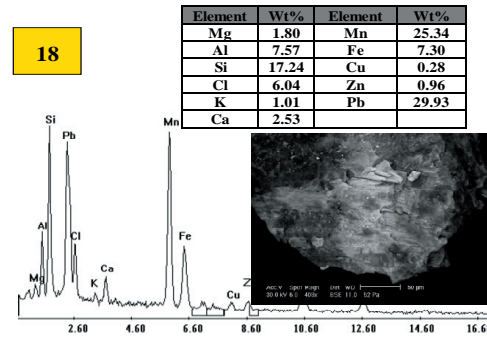


Fig. 18: BSE image, EDX analysis of Coronadite crystal from altered granite

Coronadite ($\text{PbMn}_8\text{O}_{16}$)

The manganese mineral present in the dendrites was found to be coronadite, $\text{PbMn}_8\text{O}_{16}$, which is one of hollandite-group minerals: hollandite, $\text{BaMn}_8\text{O}_{16}$ and cryptomelane, $\text{KMn}_8\text{O}_{16}$ (Potter and Rossman, 1979). It is an admixture between Mn, and Pb oxides with impurities of Fe, Al, S and Zn (Betekhtian, 1973). It has black colour and sub-metallic to dull luster with massive and botryoidal structure (Fig. 18). EDX analyses clarify that this mineral is mainly composed of Mn and Pb with K, Al, Si, Fe and Cl due to its incorporation with iron stained k-feldspar and cotunite. Cu and Zn are also recorded with different proportions (Fig. 18). On the other hand, the presence of uranium with Pb shows that U is associated with coronadite mineralization and that Pb in coronadite may result from the decay of uranium (i.e. radiogenic). Ibrahim et al. (2002 and 2004); Mansour (2005) and Mansour et al. (2009) found Mn and Pb minerals (i.e. kasolite, Mn-Franklinite and Pyrolusite) in the shear zone and Khour Abalea of Abu Rusheid area and they are considered Abu Rusheid area as a suitable environment for producing coronadite.

Galena (PbS)

Galena is found in association with sphalerite, pyrite, and other sulfides. Lead grey

galena grains with sub-metallic luster occur with appreciable amounts. Occurrence of lead and zinc sulphide may be of low-intermediate or high temperature origin (Deer et al., 1992). EDX analyses show that galena mainly contain Pb and S and present in association with and/or as inclusion in k-feldspar (Fig. 19).

Fluorite (CaF_2)

Fluorite occurs as discrete grains or in association with other minerals which occur as inclusions in fluorite such as kasolite, uraniferous xenotime and cotunite. The energy dispersive X-ray (EDX) spectrums indicate the presence of radioactive elements concentrated within some radioactive and accessory minerals such as uranophane, kasolite and uraniferous xenotime (Figs. 20-22). The accessory minerals contain more than 80 % of uranium, while 20 % of uranium is associated with the essential rock forming minerals (Pagel, 1982). Thus, radioactive contents in the studied granitic rocks can be attributed to the presence of the previous radioactive and accessory minerals. Uranium content in the studied uraniferous xenotime reach up to 21.67wt% in association with heavy rare earths, Y, P, Al, Si, K, Ca and Fe (Fig. 23). Most of these minerals are also found as inclusions in k-feldspar causing their metamictization and alteration. Sphalerite occurs as inclusion in k-feldspar confirming the

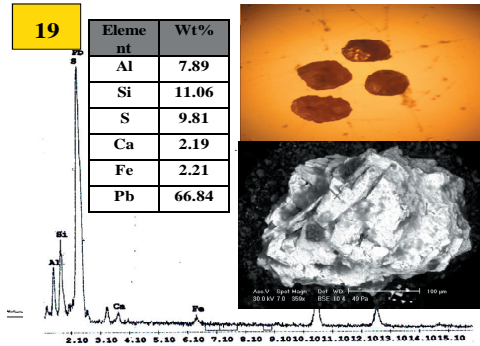


Fig. 19: Binocular photomicrograph, BSE image, EDX analysis of Galena crystal from altered granite

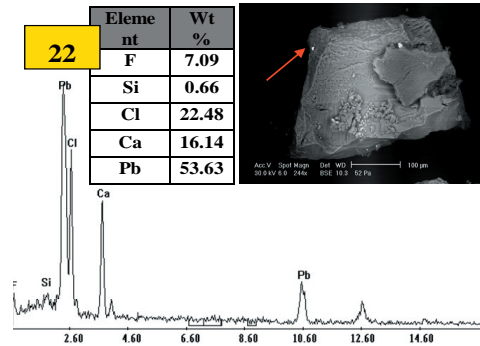


Fig. 22: BSE image, EDX analysis of Cotunitite in fluorite crystal from altered granite

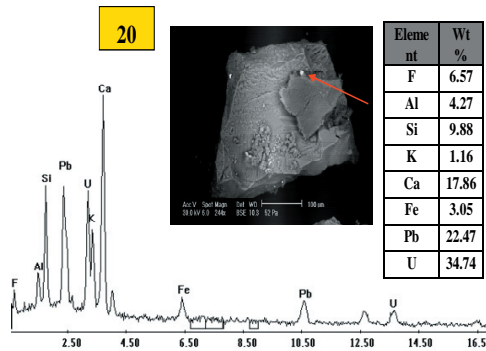


Fig. 20: BSE image, EDX analysis of Kasolite in fluorite crystal from altered granite

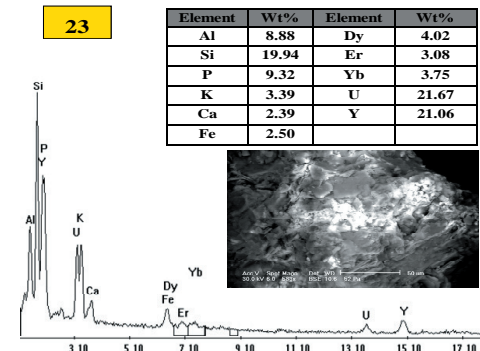


Fig. 23: BSE image, EDX analysis of uraniferous xenotime from altered granite

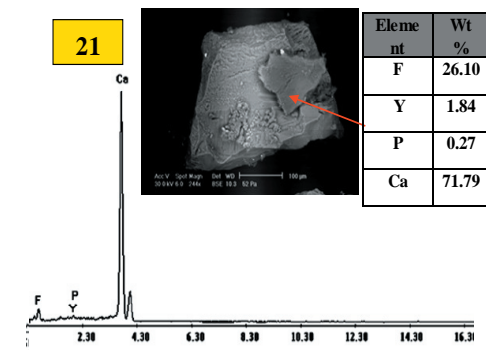


Fig. 21: BSE image, EDX analysis of fluorite crystal from altered granite

rule of hydrothermal processes in alteration of the studied granite and Sulphur content in acidification of the mineralizing solutions in granite and stream sediments (Fig. 24).

Amazonite

The studied gattarian granites are characterized by the presence of appreciable amounts of amazonite (green variety of microcline) crystals. Amazonite occurs as disseminated bluish green crystals within the gattarian granites. ESEM analysis shows its typical composition K, Si and Al are the main components (Fig. 25).

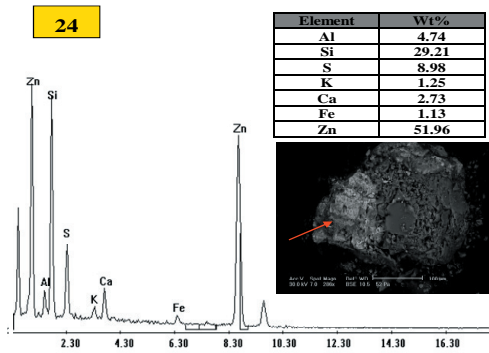


Fig. 24: BSE image, EDX analysis of Sphalerite crystal on K-Feldspare

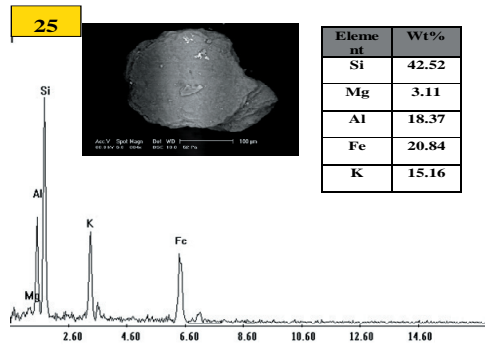


Fig. 25: BSE image, EDX analysis of Amazonite crystal from altered granite

Geochemical Characteristics of the Altered Granites

The distributions of the major, trace and REEs in the altered zones of Gattar granites (Table 1) yielded some useful information on rock/fluid interaction characteristics, in addition to the physicochemical conditions of the system. During the hydrothermal alteration, nearly all the major and trace elements were mobilized due to dissolution or replacement of the main components and accessory minerals and new-formation of mineral phases.

The different types of hydrothermal alterations could be determined by the well-known alteration diagrams as the normative Qz-Ab-Or of Stemprok (1979), Q-P diagram of Debon and Le Fort (1983), Na₂O-K₂O variation diagram (Cuney, 1987). Creasy (1959) classified the hydrothermally altered rocks as argillic facies (characterized by any member of the kaolinite group) and K-silicate facies (characterized by muscovite-biotite and K-feldspar). The argillic facies was classified by Meyer and Hemely (1967) as advanced argillic (kaolinite and montmorillonite replacing plagioclases) and intermediate argillic (all the feldspars are converted to dickite and kaolinite).

The normative Qz-Ab-Or ternary diagram after Stemprok (1979) shows that altered

Table 1: Chemical composition of Gattar altered granites, Eastern Desert, Egypt

Oxide %	Altered granite			Element ppm	Altered granite			Element ppm	Altered granite			Ratios	Altered granite		
	N9	N9a	N9b		N9	N9a	N9b		N9	N9a	N9b		N9	N9a	N9b
SiO ₂	58.78	66.95	50.61	Ba	49	38	60	Bi	4.14	3.13	5.15	La/Yb _n	0.3	0.2	0.3
Al ₂ O ₃	20.28	16.48	24.08	Co	3.8	2.9	4.7	V	230.9	221.0	240.8	La/Sm _n	0.6	0.6	0.6
TiO ₂	0.13	0.10	0.17	Cs	21.9	17.8	26	La	15.1	10	18.2	Gd/Yb _n	0.4	0.4	0.5
Fe ₂ O ₃ ^t	5.93	4.49	7.38	Ga	99.42	89.41	109.43	Ce	52.95	94.42	60.3	Sr/Eu	250	409	182
MgO	0.63	0.48	0.78	Hf	12.88	9.87	15.89	Pr	8.3	6.2	10.3	Eu/Sm	0.01	0.01	0.02
CaO	5.14	3.72	6.55	Nb	115.51	100.50	130.52	Nd	37	26.9	45.1	Y/Ho	22.64	31.13	19.58
Na ₂ O	0.77	0.63	0.91	Rb	893.3	873.2	913.4	Sm	15.9	10.8	18.1	LREE/HREE	0.85	0.79	0.88
K ₂ O	7.14	5.93	8.36	Sr	241.8	231.7	251.9	Eu	0.2	0.1	0.3	Ce/Ce*	1.24	1.48	1.17
MnO	0.17	0.17	0.18	Sr	50	40.9	60.1	Gd	19	15.9	21.1	Eu/Eu*	0.0	0.0	0.1
P ₂ O ₅	0.02	0.01	0.03	Ta	10.1	7.4	13.2	Tb	5.1	4	6.3	Zr/Hf	17.61	20.94	14.91
L.O.I.	0.14	0.14	0.14	Tb	33.2	19.1	37.3	Dy	40.4	33.3	44.7	Nb/Ta	11.44	13.58	09.89
				U	359.7	339.6	379.8	Ho	10.2	7.1	12.3	U/Tb	10.83	11.67	1018
				V	55	48.9	62.1	Er	32.6	25.5	38.7	Ba/Sr	0.98	0.93	1.00
				W	15.8	10.7	20.9	Sm	15.9	10.8	18.1	Ba/Rb	0.07	0.04	0.07
				Zr	226.8	206.7	236.9	Tm	5.6	4.5	6.5	Rb/Sr	17.87	21.35	15.20
				Mo	27.35	20.34	34.36	Yb	34.8	28.7	36.9	t1	1.25	1.40	1.23
				Cu	161.4	155.3	166.5	Lu	5.2	4.1	6.2	t3	1.12	1.18	1.13
				Pb	2282.38	2272.37	2292.39	REE	282.35	220.04	325	TE _{1,3}	1.18	1.28	1.18
				Zn	6566.9	6556.8	6576.7	LREE	129.45	96.94	152.3	t4	1.11	1.15	1.04
				Ni	2.7	2.0	3.4	HREE	152.9	123.1	172.7	TE _{1,4}	1.15	1.23	1.23

T1, T3, T4 AND T ARE CALCULATED ACCORDING TO IRBER (1999) , (-): NOT DETERMINED.

granite samples having high K_2O content are shifted towards potassic trend and one sample shows imprints of greisenization as indicated by Manning (1981), (Fig. 26).

The Na_2O - K_2O binary diagram after Cuney et al., (1989), indicate that all samples with high Na_2O contents (desilicified samples) are shifted towards albite during Na-metasomatism, albitization proceeds through the replacement of Na^+ for K^+ and Ca^{2+} of the pre-existing feldspars but silicification results in an increase of SiO_2 at the expense of other major elements and accompanied with increasing of some trace elements such as Zr, Ba and Rb.

By using the Na_2O - K_2O variation diagram of Cuney et al., (1989) the studied altered granites samples fall in desilicification, K-metasomatism and silicification fields (Fig. 27).

Meyer and Hemely (1967) classified the alteration types of K-silicate into; (i) propylitic (containing epidote-chlorite alteration), (ii) sericitic (containing k-feldspars that converted into sericite) and (iii) potassic (characterized by the alteration of plagioclase into K-feldspar or mafic minerals into muscovite) subtypes. It is clear that all samples fall in the field between sericite and argillicfacies (due to sericitization processes) suggesting overprints of different types of alteration on these rocks (Fig. 28).

(Na_2O+CaO) - Al_2O_3 - K_2O ternary diagram of Nesbitt and Young (1989) shows that all altered granites samples are parallel to advanced weathering trend, which its initial trend parallel to the K_2O - Al_2O_3 side-line of the diagram (Fig. 29).

The original rock alteration could be determined depending on Al_2O_3 - CaO + Na_2O - K_2O diagram of Nesbitt and Young (1984). It shows clear discrimination between slightly, moderately and deeply alterations processes (Fig. 30). The ideal feldspar weathering line (IWL), which parallels the Al_2O_3 , CaO + Na_2O trend towards illite, is due to post-depositional K-enrichment in clay fraction (Fedo et al., 1995), suggests K-metasomatism (Fedo et al.,

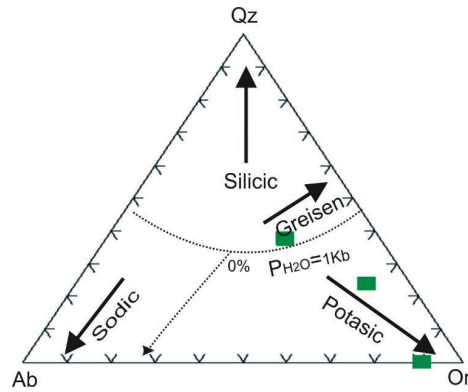


Fig. 26: Normative Qz-Ab-Or ternary diagram

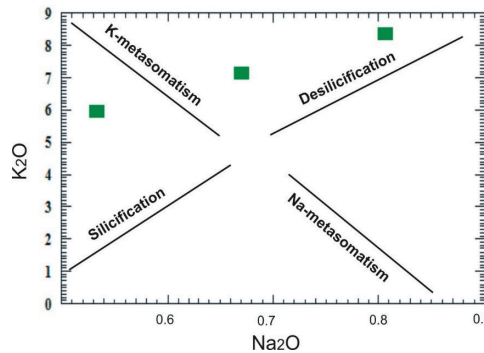


Fig. 27: Na_2O - K_2O variation diagram of Cuney (1987)

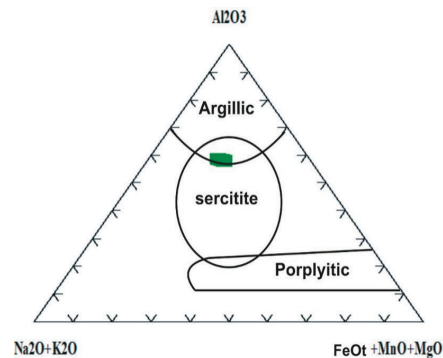


Fig. 28: Al_2O_3 - (Na_2O+K_2O) - $(FeOT+MnO+MgO)$ ternary diagram (Meyer and Hemely, 1967)

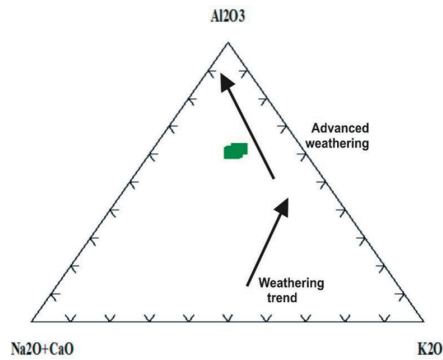


Fig. 29: $Al_2O_3-(Na_2O+CaO)-K_2O$ ternary diagram (Nesbitt and Young, 1989) for altered granitic rocks

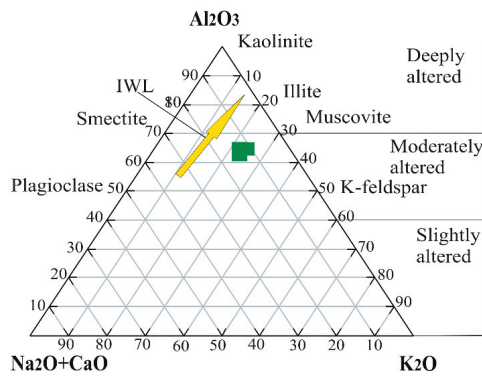


Fig. 30: $Al_2O_3-(Na_2O+CaO)-K_2O$ ternary diagram Nesbitt and Young (1989)

1997, Roser et al., 2002). Samples of Gattar altered granites indicate moderate to strong alterations and plot along the illite trend on $Al_2O_3, CaO+Na_2O$ axis, suggesting K-metasomatism.

Chemical variations in the altered rocks

Chemical variations in the altered granite cause losses and gains of some elements. Mass balance calculations were carried out in order to quantify the actual loss or addition of major and trace components during K-metasomatism. The numerical values of element

enrichment and depletion accompanying the present types of alteration are shown in Table (2). The variations of the geochemical of the altered syenogranite are caused by the loss and gain of some elements. To understand the geochemical behavior of elements in the altered granites, it is recommended to normalize the pattern of such altered rocks to its corresponding fresh granite (syenogranite). After that, the reference granite pattern becomes flat at unity and the relative depletion or enrichment are given by the deviations on both sides of the reference line. Geochemistry of major oxide is discussed in terms of gains (positive) and losses (negative) of these elements during the alteration of granites. Generally, loss and gain calculations indicate that the altered samples exhibit increasing in total iron, K, Mn, Al, Ca and Mg and decreasing in Na, P, Si, L.O.I. and Ti (Fig. 31), in addition to the elevated Cu, Co, Pb, Cs, Y, Ga, Hf, Sn, V, Nb, Rb, Ta, Th, U, Tl, Zr, W, Zn and the depleted Ba, Sr and Ni contents (Fig. 32).

The behavior of these trace elements might be governed by physicochemical conditions of the hydrothermal solutions. The enrichment of Al and K could be related to the sericitization of feldspars, while the enrichment of Fe_2O_3 and MgO were resulted from the hematization and chloritization of biotite.

High Mn and Pb contents could be attributed to the presence of kasolite, cotunite, coronadite and galena. The depletion in P_2O_5 and LREEs might be controlled by the probable dissolution of monazite, and migration of these elements from altered granites to their associating stream sediments.

U and Th additions may be controlled by the presence of uranophane, Kasolite and other accessory minerals. The HREEs enrichment could be due to the occurrence of zircon and xenotime in mineral association (Fig. 33), while the elevated contents of chalcophile element e.g. Cu, Mo, and Zn are diagnostically high in the altered granite due to their incorporation in sphalerite and other sulphides.

Table 2: Averages of mass balance (%) of the studied samples

Major Oxides	N9			N9a			N9b			Trace	N9			N9a			N9b			REE	N9			N9a			N9b		
	N9	N9a	N9b	N9	N9a	N9b	N9	N9a	N9b		N9	N9a	N9b	N9	N9a	N9b	N9	N9a	N9b		N9	N9a	N9b	N9	N9a	N9b	N9	N9a	N9b
SiO ₂	-21.26	-10.31	-32.20	Ba	-87.07	-89.97	-84.17	La	-84.35	-89.64	-81.14																		
Al ₂ O ₃	-34.00	-51.50	-16.50	Co	90.00	45.00	135.00	Ce	-43.42	-54.11	-35.56																		
Fe ₂ O ₃	50.00	21.89	78.11	Cs	21.90	17.80	26.00	Pr	22.06	-8.82	51.47																		
MgO	266.05	177.16	355.56	Ga	99.42	89.41	109.43	Nd	72.49	25.41	110.26																		
CaO	429.90	283.51	575.26	Hf	12.88	9.87	15.89	Sm	165.00	80.00	201.67																		
Na ₂ O	142.31	84.62	200.00	Nb	230.03	187.14	272.91	Eu	-55.56	-77.78	-33.33																		
K ₂ O	-81.92	-85.21	-78.64	Rb	507.69	494.01	521.36	Gd	136.02	97.52	162.11																		
TiO ₂	57.96	31.19	84.96	Sn	241.80	231.70	251.90	Tb	521.95	387.80	668.29																		
P ₂ O ₅	-70.00	-81.67	-51.67	Sr	-53.70	-62.13	-44.35	Dy	703.18	562.03	788.67																		
MnO	330.00	320.00	340.00	Ta	10.10	7.40	13.20	Ho	871.43	576.19	1071.43																		
LOI	-83.72	-83.72	-83.72	Th	95.29	12.35	119.41	Er	990.30	752.84	1194.31																		
				Tl	4.84	3.83	5.85	Tm	998.04	782.35	1174.51																		
				U	7094.00	6692.00	7496.00	Yb	1303.23	1057.26	1387.90																		
				V	266.67	226.00	314.00	Lu	664.71	502.94	811.76																		
				W	15.80	10.70	20.90																						
				Zr	40.87	28.39	47.14																						
				Mo	1267.50	917.00	1618.00																						
				Cu	2590.00	2488.33	2675.00																						
				Pb	10274.45	10228.95	10319.95																						
				Zn	11030.34	11013.22	11046.95																						
				Ni	-66.25	-75.00	-57.50																						
				Bi	4.14	3.13	5.15																						
				Y	524.05	497.30	550.81																						

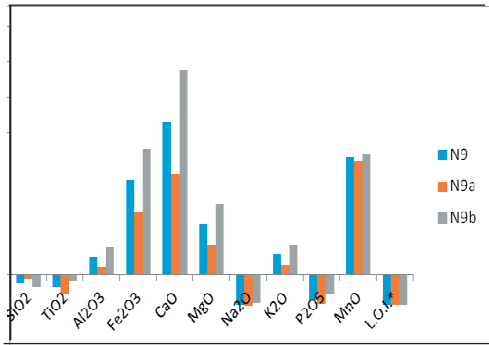


Fig. 31: Histogram showing the depletion and enrichment of major oxides of altered granite

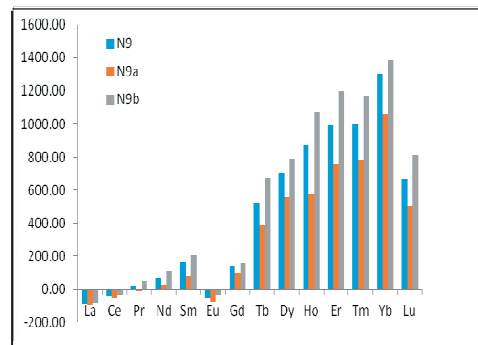


Fig. 33: Histogram showing the depletion and enrichment of REEs of altered granite

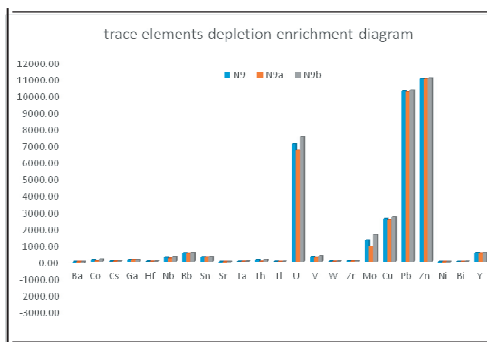


Fig. 32: Histogram showing the depletion and enrichment of trace elements of altered granite.

Rb increased with increasing of K-feldspars, sericite and muscovite. Ekwere (1985) suggested that Rb concentration increased in liquids rich in volatile components, being concentrated during the late magmatic differentiation. The remarkable depletion in the content of Ba and Sr is due to breakdown of their host feldspars. Ni depletion may be related to the formation of secondary chlorite.

Fractionation of Isovalents

The fractionation of elements, which are similar to each other in terms of ionic radius and charge is regarded to be sensitive to

changes in melt composition during magma differentiation (Bau, 1996, 1999 and Pan, 1997), Y/Ho chondrite ratio is 28 (Anders and Grevesse, 1989).

Complexation with fluorine is the major cause of Y/Ho values >28, in contrast to Y/Ho values <28 indicating complex formation with bicarbonate (Bau and Dulski, 1995). The studied altered granite Y/Ho values suggest complex formation with fluorine and bicarbonate, where Y/Ho values are >28 in sample N9b and <28 in samples N9a and N9c, which is confirmed by the presence of fluorite and calcite mineralization in these granites.

Dostal and Chatterjee (2000) indicated that Zr/Hf ratios fall in a narrow range of 33–40. Deviation from the range was rare and usually attributed to metasomatism or intense fractionation of accessory minerals. The studied granite samples have reduced Zr/Hf ratios and shift towards smaller values (<20), indicating that these rocks are affected by strong magmatic hydrothermal alteration in highly fractionated silicate melt (Irber, 1999).

Sr/Eu chondritic ratio is 139 (Anders and Grevesse, 1989). In the studied samples, the Sr/Eu ranges from 182 to 409, this indicates highly fractionated nature due to high alteration processes. It identifies non-CHARC behavior in aqueous system because of the fractionation of highly charged ions, which form strong chemical complexes.

Also, the non-chondritic ratios for Nb/Ta (19.58-31.13), La/ Nb (0.10-0.14) and La/ Ta (1.35-1.50) for the altered granites clarify highly differentiated nature of the studied altered granites. The chondritic ratios are 17.6 ± 1 for Nb/Ta, (0.96-1) for La/Nb and (16-18) for La/Ta (Jahn et al., 2001).

Rb/Sr ratio increases with differentiation; this is due to the fact that Sr is depleted in the liquid magma as a result of crystallization of feldspar, while Rb is enriched in liquid phase. The Studied altered granite has high Rb/Sr ratios (15.20-21.35) indicating highly evolved granitic rocks.

Uranium Distribution

K-metasomatic and episyenitization alterations in the analyzed samples are correlated with uranium enrichment (339.6-379.8), suggesting that K-metasomatism is more correlated to the uranium mineralization. The high average uranium and thorium contents when compared with the crustal values of 1.80 ppm U and 7.20 ppm Th (Mason and Moore, 1991) indicate the enrichment of these elements in the Gattar granite (Fig. 34). Uranium also indicates positive correlation with most trace elements as it is shown on Figures (35-44).

REE Tetrad Effect

The average of total REE contents (Table 1) of the studied altered granites were 275.5, suggesting that these granites were enriched in REE relative the international range (250-270) of Hermann (1970). The LREE are depleted and the HREE including Y are enriched.

The low LREE/HREE ratio indicates the HREEs enrichment in granites underwent K-metasomatism. The Chondrite-normalized patterns of the analyzed samples (Fig.45) exhibit moderate fractionation of the L, where $(La/Sm)_n \sim 0.6$, while the HREE are less fractionated $(Gd/Yb)_n$ (0.4 to 0.5). The altered granite show faint fractionated wing shape pattern $(La/Yb)_n = 0.2-0.3$. REEs patterns show positive Ce anomalies indicating low O_2 fugacity at the magma source (Constantopoulos, 1988). The negative Eu anomaly is deep with a value of $Eu/Eu = 0.3$ and $Eu/Sm = 0.01-0.02$. This type also belongs to the first group of Cullers and Graff (1984) with strong negative Eu anomaly.

The tetrad effect describes the division of the REE into four segments that correspond to quarter, half, three-quarters and complete filling of the 4f electronic shell. This phenomenon is traditionally explained in terms of electronic repulsion energy with the successive filling of the 4f shell. However, Kawabe et al. (1999) noted that the type of ligand involved in the lanthanides complexing may

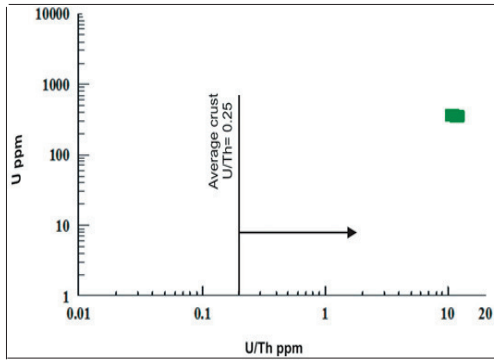


Fig. 34: U-U/Th diagram showing the enrichment of uranium in the granite of G. Gattar

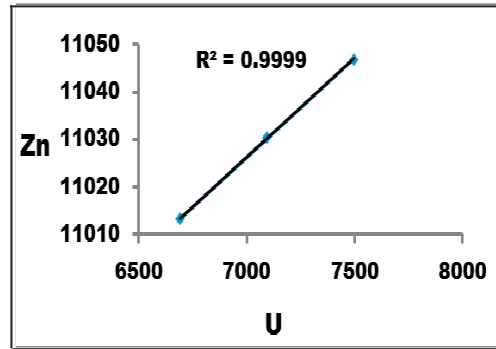


Fig. 37: U-Zn (ppm) correlation diagram

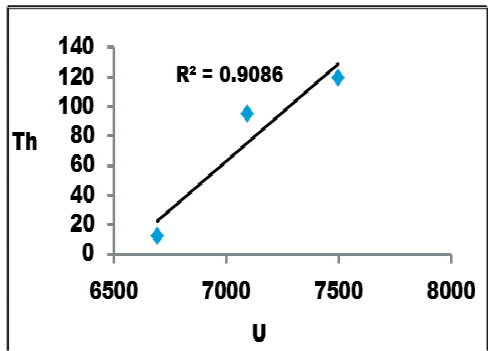


Fig. 35: U-Th (ppm) correlation diagram

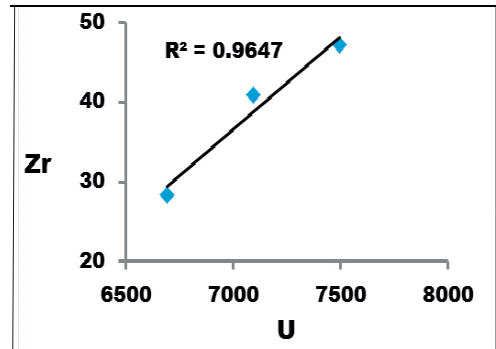


Fig. 38: U-Zr (ppm) correlation diagram

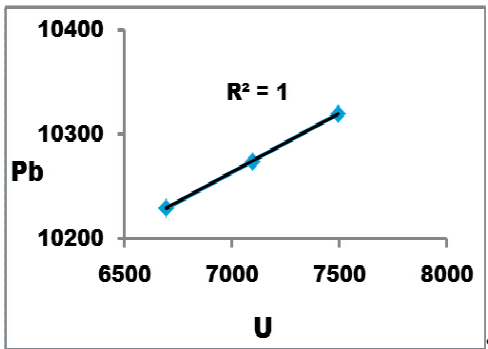


Fig. 36: U-Pb (ppm) correlation diagram

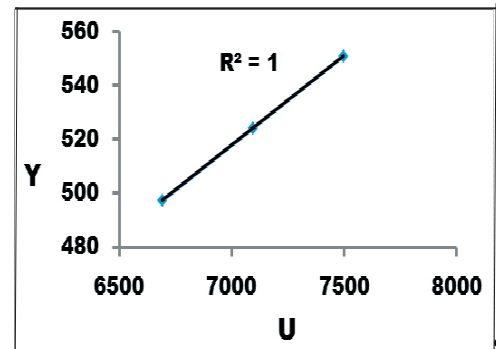


Fig. 39: U-Y (ppm) correlation diagram

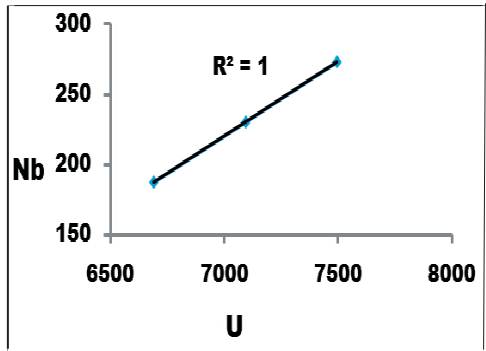


Fig.(40) U-Nb (ppm) correlation diagram

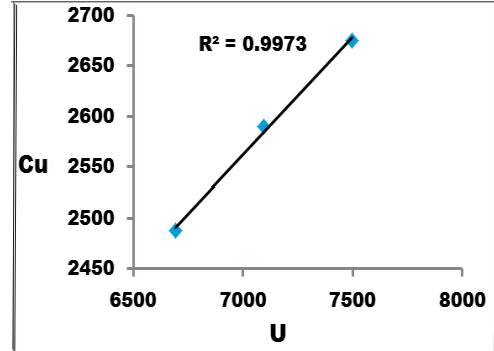


Fig. 43: U-Cu (ppm) correlation diagram

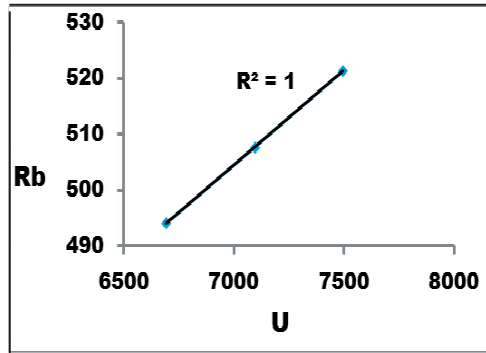


Fig. 41: U-Rb (ppm) correlation diagram

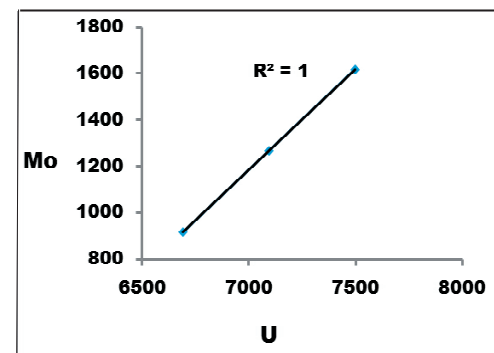


Fig. 44: U-Mo (ppm) correlation diagram

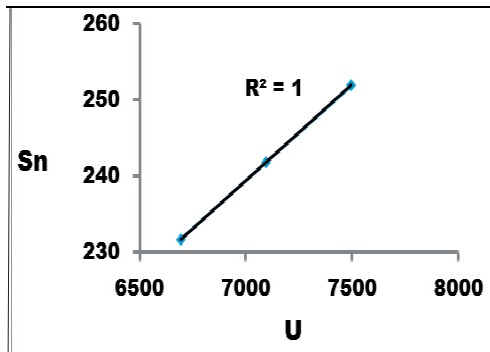


Fig. 42: U-Sn (ppm) correlation diagram

enhance or reduce the inter-electronic repulsion, and thereby affect the behavior of the REE in the geochemical systems. The modern advances indicate that the REE budget of the hydrothermal fluids mobilize under particular conditions of metasomatic alteration (Michard, 1989). The REE mobility is controlled by pH, high water/rock ratios and abundant complexing ions CO_3^{2-} , F^- , Cl^- , PO_4^{2-} , SO_4^{2-} , (Hass et al., 1995).

The present work introduces the tetrad effect as a tool for better understanding of the physical-chemical conditions prevailed during the metasomatic alteration in Gattar altered granites.

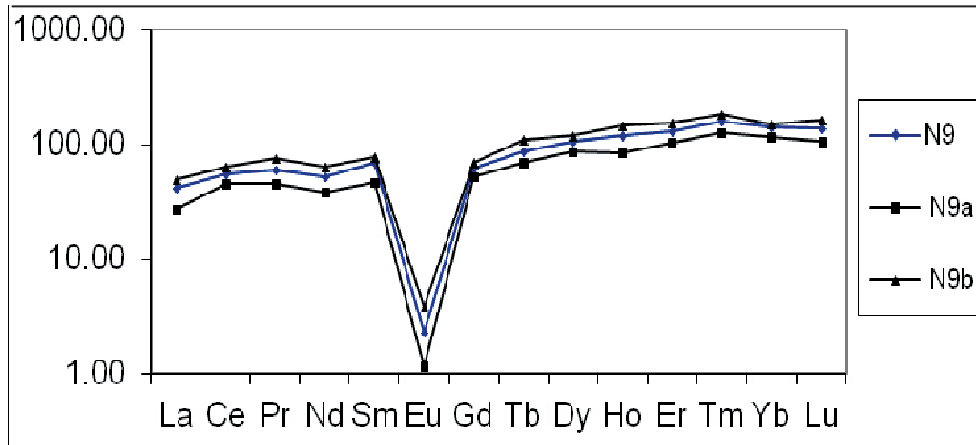


Fig. 45: Chondrite- normalized REE diagram (Boynton, 1984) for the investigated altered granites

The values of tetrad effect were calculated according to the quantification method of Irber (1999):

$$t1 = (Ce/Ce^* \times Pr/Pr^*), t3 = (Tb/Tb^* \times Dy/Dy^*), t4 = (Tm/Tm^* \times Yb/Yb^*)$$

$$\text{Degree of the tetrad effect } T_{1,3} = (t1 \times t3)^{0.5}$$

A REE pattern that does not show a tetrad effect has values of $TE_{1,3} < 1.1$. The M-shaped pattern shows $TE_i > 1.1$ and the W-shaped $TE_i < 0.9$.

The metasomatized Gattar granites display strong convex (M-type) first, third and fourth tetrad segments (T_1 , T_3 and T_4), with values ranging between 1.23 and 1.40 for T_1 , 1.12 and 1.18 for T_3 , 1.04 and 1.15 for T_4 . REE patterns clarify that T_1 is stronger than T_3 and T_4 (Fig. 36). Sample N9b shows the highest tetrad effect values suggesting the role of fluoritization and fluorine ligands in fractionation of isovalents and the resulting tetrads. The lowest tetrad values noticed in most samples are recorded in T_4 . The index of tetrad effect intensity, $TE_{1,3}$ and $TE_{1,4}$ are higher than 1.10 ranging from 1.18 to 1.28 and $TE_{1,3}$ from 1.15 to 1.23 which implies that there was an

interaction between melt and water-haloid-rich fluid when these granites are crystallized from magma.

DISCUSSION

One of the main problems to the presentation of a model for genesis of uranium mineralization at Gattar area is the absence of suitable age framework for different stages of alterations and mineralizations that taken place in the mineralized zone. However, it is suggested that, mineralization of Gattar granite would be taken place through several steps.

The first step was the generation from highly evolved peraluminous calc-alkaline magmas enriched in compatible (LIL) and HFS-elements, which were developed in a within-plate tectonic setting (Roz, 1994; Shalaby, 1996; Nosseir, 1996; Abdel-Monem et al., 1998; El-sayed, 2003; El Feky, 2011; Shalaby et al., 2015). Other features include high differentiation index, high Rb/Sr ratios and low Ba/Rb ratios. High Rb/Sr ratios and low Ba/Rb ratios can be used as indicators for post-magmatic alteration and mineralization (Abdel-Monem et al., 1998).

Extensive alteration of the host younger granites in the mineralized zone was observed. Different types of hydrothermal alteration accompanying the uranium mineralization are mainly represented by silicification, kaolinization, chloritization, sericitization, fluoritization, hematitization, desilicification, in addition to carbonitization, muscovitization, albitization, pyritization. It can be concluded that the main mineralization solution was firstly acidic during silicification and kaolinization resulting in the liberation of uranium and other metallic elements from the structure of the primary accessory minerals as well as biotite, chlorite and epidote and concentrate them in the mineralizing solutions. The deep circulating solutions were heated by the action of an elevated geothermal gradient from radioactive decay of U, Th and K in granites (Birch, 1954; Fehn 1978; Shrier and Parry, 1982; Min et al., 1999) and also by the effect of the intrusion of basic dykes (Roz, 1994). Therefore, dykes may have some contributions in uranium mineralization in addition to providing a possible redox boundary (chemical trap for U-bearing solutions). Also, the presence of secondary uranium minerals near the contact with mafic dykes reflects the effect of mafic dykes in fixing uranium from solution in secondary minerals (Pagel, 1982). The hydrothermal solutions used the pathway of the shear zone while moving and have further leached uranium and other elements from the host rock and became mildly acidic mineralizing fluids due to the interaction with the host rock (Min et al., 1999). The abundance of vein fluorite and regional occurrence of carbonates and minor calcite veining in the mineralized zone suggest that both fluorine and CO₂-rich fluids were possible. Mahdy (1998) mentioned that the main mineralizing solutions were carbonates rich while Helmy (1999) inferred from the common association of uranium minerals and fluorite, that uranium was transported as uranium fluoride complex. Mahdy (1998), stated that any genetic model of uranium mineralization in Gattar area could be evolved by the effect of ascending hydrothermal activity, car-

rying uranium as well as other important trace elements (e.g. REEs) from a deeper source. These solutions may be of magmatic origin or heated by circulation in convection cells. The association of rare metal and uranium mineralization in the studied altered granites indicate that the main mineralizing solutions could be enriched in these elements.

CONCLUSION

Gabal Gattar batholith is located among the basement rocks of the northern part of the Eastern Desert, Egypt. It is the most important highly evolved peraluminous granitic pluton hosting U-mineralization. Petrological and geochemical studies on the new discovered uranium occurrence indicate that desilicification, k-metsomatism and fluoritization are the main alteration features. Alteration processes of Gattarian granites were accompanied by unusual REEs patterns and non-CHARC behavior of isovalents. Loss and gain mass balance calculations indicate that the altered samples, generally, exhibit an increase in total iron, K, Mn Al, Ca and Mg and decrease in Na, P, Si, L.O.I. and Ti, in addition to the elevated Cu, Co, Pb, Cs, Y, Ga, Hf, Sn, V, Nb, Rb, Ta, Th, U, Tl, Zr, W, Zn and the depleted in Ba, Sr and Ni contents. Good correlation between uranium and some trace and rare earth elements clarify the mobilization and precipitation of these elements during the physico-chemical changes associating alteration processes. The mineral associations in the studied altered granite are mainly represented by uranophane, kasolite, cotunite, coronadite, galena, fluorite and amazonite.

REFERENCES

- Abdel-Monem, A.; El-Amin, H.M.; El-Afandy, A.H.; Hussein, H.A. and Abdel-Aty, M.E., 1998. Petrological and geochemical characteristics of some younger granites bearing uranium mineralization: Recognition criteria of uranium province in Egypt. Proc. Egypt. Acad. Sci., 48, 213-270.

- Africano, F.; Van Rompaey, G.; Bernard, A.; Le Guern, F., 2002. Deposition of trace elements from high temperature gases of Satuma-Iwojima volcano Earth. *Planet and Space*, 54, 275-286.
- Ammar, A.A., 1973. Application of aerial radiometry to the study of the geology of Wadi El Gidami area, Eastern Desert, Egypt (with aeromagnetic application), Ph.D. Thesis, Fac. Sci., Cairo Univ., Egypt, 424p.
- Anders, E. and Grevesse, N., 1989. Abundances of the elements: Meteoritic a solar. *Geochim. Cosmochim. Acta.*, 53, 197-214.
- Bau, M., 1996. Controls on the fractionation of iso-valent trace elements in magmatic and aqueous systems: evidence from Y/Ho, Zr/Hf and lanthanide tetrad effect. *Contrib. Mineral. Petrol.*, 123, 323-333.
- Bau, M., 1999. Scavenging of dissolved yttrium and rare earths by precipitating iron oxyhydroxide: Experimental evidence for Ce oxidation, Y-Ho fractionation, and lanthanide tetrad effect. *Geochim. Cosmochim. Acta*, 63, 67-77.
- Bau, M. and Dulski, P., 1995. Comparative study of yttrium and rare-earth element behaviours in fluorine-rich hydrothermal fluids, *Contrib. Mineral. Petrol.*, 119, 213-223.
- Betekhtian, A., 1973. A course of mineralogy. (English version), Peace Pub, Moscow, USSR, 64.
- Birch, F., 1954. Heat from radioactivity. In: Fual, Henry (ed.): *Nuclear Geology*, New York, John Wiley, 148-174.
- Constantopoulos, J., 1988. Fluid inclusion and rare earth elements geochemistry of fluorite from South Central Idaho. *Econ. Geol.*, 83, 626-636.
- Creasy, S.C., 1959. Some phase relations in hydrothermal altered rocks of porphyry copper deposit. *Jour. Econ. Geol.*, 54, 351-373.
- Cullers, R.L. and Graf, J.L., 1984. Rare earth elements in igneous rocks of the continental crust: Intermediate and silicic rocks ore petrogenesis. In: Henderson, P. (ed.): *Rare Earth Element Geochemistry*, Elsevier, Amsterdam, 275-316.
- Cuney, M., 1987. *Metallogenesis of Uranium Deposits*. IAEA, Vienna.
- Cuney, M.; Leorty, J.; Valdiviezo, P.A.; Daziano, C.; Gamba, M.; Zarco, J.; Morello, O.; Ninci, C. and Molina, P., 1989. Geochemistry of the uranium mineralized Achala Granitic Complex, Argentina: Comparison with Hercynian peraluminous leucogranites of Western Europe. *Metallogenesis of Uranium Deposits*, 211-232. IAEA-Tc-452/6, Vienna.
- Debon, F. and Le Fort, P.A., 1983. chemical-mineralogical classification of common plutonic rocks and associations. *Trans. R. Soc. Edinburgh Earth Sci.*, 73, 135-149.
- Deer, W.A.; Howie, R.A. and Zussman, J., 1992. *An Introduction to The Rock Forming Minerals*, 2nd ed., Longman, London, 696p.
- Dostal, J. and Chatterjee, A.K., 2000. Contrasting behavior of Nb/Ta and Zr/Hf ratios in a peraluminous granitic pluton (Nova Scotia, Canada). *Chem. Geol.*, 63, 207-218.
- Ekwere, S.J., 1985. Li, F and Rb contents and Ba/Rb and Rb/Sr ratios as indicators of post-magmatic alteration and mineralization in the granitic rocks of the Banke and Ririwai younger granite complexes, North Nigeria. *Mineral. Deposita.*, 20, 89-93.
- El-Feky, M.G., 2011. Mineralogy, M-type tetrad effect and radioactivity of altered granites at the G. Abu Garadi shear zone, central Eastern Desert, Egypt. *Chin. Jour. Geochem.*, 30, 153-164.
- El-Kassas, I.A., 1974. Radioactivity and geology of Wadi Atalla area, Eastern Desert of Egypt. Ph.D. Thesis, Fac. Sci., Ain Shams Univ., Egypt.
- El-Kholy, D.M.; El-Husseiny, M.O.; Saleh, W.H. and El-Zalaky, M.A., 2012. Remote sensing, geology and geochemistry on the GVIII uranium mineralization, Gabal Gattar, North Eastern Desert, Egypt. *Nuclear Sciences Scientific J.*, 1, 69-84.
- El-Taher, M.A., 1985. Radioactivity and miner-

- alization of granitic rocks of El-Erediya occurrence and comparison of El-Missekat-Rie Garra occurrence, Eastern Desert, Egypt. Ph.D. Thesis, Fac. Sci., Al-Azhar Univ., Egypt, 133p.
- El-Sayed, M.M.; Shalaby, M.H. and Hassanen, M.A., 2003. Petrological and geochemical constraints on the tectonomagmatic evolution of the late Neoproterozoic granitoids suites in Gattar area, North Eastern Desert, Egypt. *N. Jb. Miner. Abb.*, 178, 239-275.
- Fedo, C.M.; Nesbitt, H.W. and Young, G.M., 1995. Unraveling the effects of potassium metasomatism in sedimentary rocks and paleosols, with implications for paleoweathering conditions and provenance. *Geology*, 23, 921-924.
- Fedo, C.M.; Young, G.M.; Nesbitt, H.W. and Hancher, J.M., 1997. Potassic and sodic metasomatism in the Southern Province of Canadian Shield: Evidence from Paleo proterozoic Serpent Formation, Huronian Supergroup. *Canada. Precambrian Res.*, 84, 17-36.
- Fehn, U.; Cathles, L.M. and Holland, H.D., 1978. Hydrothermal convection and uranium deposits in abnormally radioactive plutons. *Econ. Geol.*, 73, 1556-1566.
- FrondeL, C., 1958. Systematic mineralogy of uranium and thorium. *U.S. Geol. Surv. Bull.*, 1064, 400p.
- Grothaus, E.B. and Eherlich, R., 1979. Depositional environment and structural implications of the Hammamat formation, Egypt. *Ann. Geol. Surv., Egypt.*, 9, 564-590.
- Hass, J.R.; Shock, E.L. and Sassani, D.C., 1995. Rare earth elements in hydrothermal systems: Estimates of standard partial molal thermodynamic properties of aqueous complexes of the rare earth elements at high pressures and temperatures. *Geochim. Cosmochim. Acta.*, 59, 432-435.
- Heinrich, E.W., 1958. *Mineralogy and Geology of Radioactive Raw Materials*. McGraw-Hill, New York, 621p.
- Helmy, H.M. 1999. Mineralogy, fluid inclusions and geochemistry of the molybdenum-uranium-fluorite mineralization, Gabel Gattar area, Eastern Desert, Egypt. 4th intern. Conf. on Geochemistry, Alex. Univ., Egypt, 171-188.
- Herrman, A.G., 1970. Yttrium and lanthanides: In: Wedepohl (ed.): *Handbook of Geochemistry*, Springer verlag, New York, 39-57.
- Hussein, H.A.; Ali, M.M. and El-Ramly, M.F., 1982. A proposed new classification of the granites of Egypt. *Jour. Volcan. Geotherm. Res.*, 14, 187-194.
- Ibrahim, M.E.; Saleh, G.M.; Abd El-Naby, H.H.; Amer, T.; Mahmoud, F.O., Abu El-Hassan, A.A.; Ibrahim, I.H.; Aly, M.A.; Azab, M.S.; Rashed, M.A.; Khaleal, F.M. and Mahmoud, M.A., 2002. Uranium and associated rare metals potentialities of Abu Rusheid brecciated shear zone I, South Eastern Desert, Egypt. Unpublished Report, 107.
- Ibrahim, M.E.; Saleh, G.M.; Amer, T.; Mahmoud, F.O.; Abu El-Hassan, A.A.; Ibrahim, I.H.; Aly, M.A.; Azab, M.S.; Rashed, M.A.; Khaleal, F.M. and Mahmoud, M.A., 2004. Uranium and associated rare metals potentialities of Abu Rusheid brecciated shear zone II, South Eastern Desert, Egypt. Unpublished Report, 141.
- Irber, W., 1999. The lanthanide tetrad effect and its correlation with K/Rb, Eu/Eu*, Sr/Eu, Y/Ho, and Zr/Hf of evolving peraluminous granite suites. *Geochim. Cosmochim. Acta.*, 63, 489-508.
- Jahn, B.; Wu, F.; Capdevila, R.; Martineau, F.; Zhao, Z. and Wang, Y., 2001. Highly evolved juvenile granites with tetrad REE patterns: The Woduhe and Baerzhe granites from the Great Xing'an Mountains in NE China. *Lithos*, 59, 171-198.
- Kawabe, I., 1992. Lanthanide tetrad effect in the Ln³⁺ ionic radii and refined spin-pairing energy theory. *Jour. Geochem.*, 26, 309-335.
- Kawabe, I.; Ohta, A. and Miura, N., 1999. Distribution coefficient of REE between Fe oxyhydroxide precipitates and NaCl solutions affected by

- REE carbonate complexation. *Geochemistry*, 33, 161-197.
- Mahdy, A.I., 1998. Petrological and geochemical studies on younger granites and Hammamat sediments at Gatter-5 uranium occurrence, Wadi Balih, North Eastern Desert, Egypt. Ph.D. Thesis., Fac. Sci., Ain Shams Univ, Egypt, 250p .
- Manning, D.A.C., 1981. The effect of fluorine on liquidus phase relationship in the system Oz-Ab-Or with excess water at 1 kb. *Contrib. Mineral. Petrol.*, 76, 206-215.
- Mansour, G.M.R., 2005. Geological and geophysical investigations of mineralized structures in Wadi Abalea and its surroundings, Abu Rusheid area, south Eastern Desert, Egypt. Ph.D. Thesis, Fac. Sci., Mansoura Univ. (Damietta Branch), Egypt, 155p .
- Mansour, G.M.; Bamite, R.A.F. and Khaleal, F.M., 2009. Reconnaissance study on economic minerals of Wadi Nugrus stream sediments: Resources and distribution. *Sci. Jour. Fac. Sci., Minoufia Univ.*, XII., 131-160.
- Mason, B. and Moore, C.B., 1991. *Principles of Geochemistry*. 4th edition, Wiley Eastern Limited, 350p.
- Masuda, A.; Kawakami, O.; Dohmoto, Y. and Takenaka, T., 1987. Lanthanide tetrad effects in nature: Two mutually opposite type W and M. *Jour. Geochem.*, 21, 119-124.
- Meyer, C. and Hemely, J.J., 1967. Wall rock alteration in geochemistry of Ore Deposits. (ed. H.L. Barnes), New York, 166-235.
- Michard, A., 1989. Rare earth element systematics in hydrothermal fluids. *Geochim. Cosmochim. Acta*, 53, 745-750.
- Min, M.Z.; Luo, X.Z.; Du, G.S.; He, BA. and Campbell, A.R., 1999. Mineralogical and geochemical constraints on the genesis of the granite-hosted Huangao uranium deposit, SE China. *Ore Geol. Rev.*, 14, 105-127.
- Monecke, T.; Kempe, U.; Monecke, J.; Sala, M. and Wolf, D., 2002. Tetrad effect in rare earth element distribution patterns: A method of quantification with application to rock and mineral samples from granite-related rare metal deposits. *Geochim. Cosmochim. Acta*, 66, 1185-1196.
- Nesbitt, H.W. and Young, G.M., 1984. Prediction of some weathering trends of plutonic and volcanic rocks based on thermodynamic and kinetic considerations. *Geochim. et Cosmochim. Acta*, 48, 1523-1534.
- Nesbitt, H.W. and Young, G.M., 1989. Formation and diagenesis of weathering profiles. *Jour. Geol.*, 97, 129-147.
- Nossair, L.M., 1996. U-F bearing episyenitized "desilicified" granitic rocks of Gabal Gattar, North Eastern Desert, Egypt. *Proc. Egypt. Acad. Sci.*, 46, 375-396.
- Page, M., 1982. The mineralogy and geochemistry of uranium, thorium and rare-earth elements in two radioactive granites of the Vosges, France. *Min Mag.*, 339, 149-161.
- Pan, Y., 1997. Controls on the fractionation of iso-valent trace elements in magmatic and aqueous systems: evidence from Y/Ho, Zr/Hf, and lanthanide tetrad effect. A discussion of the article by M. Bau (1996). *Contrib. Mineral. Petrol.*, 128, 405-408.
- Pan, Y.M. and Breaks, F.W., 1997. Rare earth elements in fluorapatite, Separation Lake Area, Ontario; evidence for S-type granite-rare-element pegmatite linkage. *Can Mineral.*, 35, 659-671.
- Potter, R.M. and Rossman, G.R., 1979. Mineralogy of manganese dendrites and coatings. *Am. Mineral.*, 64, 1219-1226.
- Raslan, M.F., 1996. Mineralogical and beneficiation studies for some radioactive granites along Wadi Balih, North Eastern Desert, Egypt. M.Sc. Thesis, Fac. Sci., Cairo Univ., Egypt.
- Roser, B.P.; Coombs, D.S.; Korsch, R.J. and Campbell, J.D., 2002. Whole-rock geochemical variations and evolution of the arc-derived Murihiku Terrane, New Zealand. *Geol. Mag.*, 139, 665-685.

- Roz, M.E., 1994. Geology and uranium mineralization of Gabal Gattar area, North Eastern Desert, Egypt. M.Sc. Thesis, Fac. Sci., Al-Azhar Univ, Egypt, 175p.
- Salem, H.A., 2004. Geochemical, mineralogical and genesis of hydrothermal uranium mineralizations hosted by late Pan-African magmatism North Eastern Desert, Egypt, Ann. Geol. Surv. Egypt, VXXVII, 225-280.
- Salman, A.B.; Shalaby, M.H. and Nossair, L.M., 1990. U-province, north Red Sea hills, Egypt. Proceedings of the International Earth Sciences Cong. On Aegean region, Izmir, Turkey, 1, 89-107.
- Shalaby, M.H., 1996. Structural controls of uranium mineralizations at Gabal Gattar, North Eastern Desert, Egypt. Proc. Egypt. Acad. Sci., 46, 521-536.
- Shalaby, M.H.; Korany, E. and Mahdy, N.M., 2015. On the petrogenesis and evolution of U-rich granite: Insights from mineral chemistry studies of Gattar granite, North Eastern Desert, Egypt. Arab Jour. Geosci., 8, 3565-3585.
- Shrier, T. and Parry, W.T., 1982. A hydrothermal model for the North Canning uranium deposit, Owl Creek Mountains, Wyoming. Econ. Geol., 77, 632-645.
- Stemprok, M., 1979. Mineralized granites and their origin, Jour. Episodes, 3, 20-24.
- Tuttle, O.F. and Bowen, N.L., 1958. Origin of granites in the light of experimental studies in the system $\text{NaAlSi}_3\text{O}_8\text{-KAlSi}_3\text{O}_8\text{-SiO}_2\text{-H}_2\text{O}$. Geol. Soc. Amer. Mem., 74, 153p.

تمعدنية وجيوكيميائية تمعدنات اليورانيوم الجديدة عند مصب وادي الرده، شمال الصحراء الشرقية، مصر

حسام انور خميس ، اسامه عبد المنعم عبيان و نيفين صلاح عابد

تتأثر جرانيتات جبل جتار بشكل كبير بالمحاليل المصاحبة له قبل تجمد الصهير والمحاليل الحرمائية بعد تجمده. تشترك التغيرات الحرمائية مع تمعدنات اليورانيوم في صخر الجرانيت الحاوي لها. وتشمل التغيرات المعدنية المصاحبة تكون الهيماتيت، السيريستيت وكذلك ازالة السيليكا علي حساب المعادن الاصلية.

يتمثل الاحلال المعدني القلوي بتكوين معادن الميكروكلين، السيريستيت والمسكوفيت علي حساب الفلسبار القلوي والبلاجيوكليز. ويتضح بشكل عام من نتائج حسابات الفقد والاكنتساب للعناصر المختلفة اثناء التغير الصخري انه توجد زيادة في نسب الحديد الكلية، البوتاسيوم، المنجنيز، الالومنيوم، الكالسيوم، الماغنيسيوم وكذلك يوجد نقص في نسب عناصر الصوديوم، الفوسفور، السيليكا، التيتانيوم ونواتج الحرق. ايضا توجد نسب مرتفعة من عناصر النحاس، الكوبالت، الرصاص، السيزيوم، الايتريوم، الجاليوم، الهافنيوم، القصدير، الفاناديوم، النيوبيوم، الربيديوم، التانتالم، الثوريوم، اليورانيوم، الثاليوم، الزركونيوم، التنجستين والزنك، وايضا نقص في عناصر الباريوم، الاسترنشيوم والنيكل. توضح نسب الايتريوم/الهولونيوم تكوين مركبات مع الفلورين والكربونات ويؤكد ذلك وجود معادن الفلوريت والكالسيت.

الدلالة علي حدوث تغيرات حرمائية في المراحل الاخيرة للصهير هو وجود قيم غير

عادية من نسب بعض العناصر. كذلك يتضح تطور هذه الصخور من وجود نموذج غير معتاد للعناصر الأرضية النادرة والتي توجد في المراحل الأخيرة قبل تجمد الصهير والممتلئة بالاحلال المعدني البوتاسيومي وتكوين الفلوريت.

توضح العلاقة الطردية لليورانيوم بمعظم العناصر الشحيحة والأرضية النادرة التحرك المشترك لهذه العناصر مع اليورانيوم. أيضا توضح الدراسات المعدنية وجود معادن اليورانوفين، الكازوليت، الكوتونيت، الكورانديت، الجالينا، الفلوريت والامازونيت.